NJC

Accepted Manuscript

This is an *Accepted Manuscript*, which has been through the Royal Society of Chemistry peer review process and has been accepted for publication.

Accepted Manuscripts are published online shortly after acceptance, before technical editing, formatting and proof reading. Using this free service, authors can make their results available to the community, in citable form, before we publish the edited article. We will replace this *Accepted Manuscript* with the edited and formatted *Advance Article* as soon as it is available.

You can find more information about *Accepted Manuscripts* in the **Information for Authors**.

Please note that technical editing may introduce minor changes to the text and/or graphics, which may alter content. The journal's standard **Terms & Conditions** and the **Ethical guidelines** still apply. In no event shall the Royal Society of Chemistry be held responsible for any errors or omissions in this *Accepted Manuscript* or any consequences arising from the use of any information it contains.

ROYAL SOCIETY
OF CHEMISTRY

NJC

ARTICLE

Facile synthesis of magnetic carboxymethylcellulose nanocarriers for pH-responsive delivery of doxorubicin

Xuejie Guo[a,b], Li Xue[c], Weizhong Lv[a,]*, Qi Liu[b], Rumin Li[b,]*, Zhanshuang Li[b] and Jun Wang[a,b]

The design of a single nanosystem with multifunctional surface properties via selecting the appropriate materials and synthesis methods was shown to be crucial in the development of drug delivery systems. In this work, modified magnetic nanocarriers have been successfully constructed using carboxymethylcellulose as the stabilization agents through a facile one-step hydrothermal method. The modified magnetic nanocarriers exhibited high magnetic saturation of 54.6 emu g^{-1} and excellent biocompatibility which was detected by a standard MTT cell assay with L929 cell lines; the nanomaterials proved reusable for drug delivery. Subsequently, doxorubicin (DOX) were loaded onto the surface of the nanocarriers and a high loading efficiency of 92.5% was attained. The results from the release characteristics of the DOX-loaded nanocarriers demonstrated that these modified magnetic nanocarriers were highly stable at neutral pH (blood plasma) and strongly pH-responsive for drug delivery in an acid environment (tumor tissue). The as-prepared multi-functional nanocarriers showed promising potential as drug carriers to improve the therapeutic efficacy of drug.

Introduction

Chemotherapy is commonly applied for human cancer treatment via using cytotoxic anti-cancer drugs; however, the major limitations of the method are side-effects of anti-cancer drugs for normal cells and low tumor targeting, such as insufficient cellular drug uptake or local drug concentration.[1-4] To address these side-effects, various drug delivery systems have been developed for the experimental and clinical delivery of therapeutic and diagnostic agents.[5-11] Recently, multifunctional carriers based on nanotechnology have drawn significant attention as promising candidates for tumor-targeting drug delivery applications.[12-16] In particular, magnetic nanoparticles have been provided unparalleled opportunity for drug delivery carriers because of their merits, such as superior magnetic properties, biocompatibility, biodegradation, chemical stability and low toxicity.[17-20] To further achieve high accumulation and selectivity at the tumor site, organic-inorganic hybrid nanomaterials have aroused extensive interest as a class of promising candidates in the drug delivery systems.[21] For magnetic nanoparticles, selecting appropriate organic materials as surface coatings is particularly crucial for their successful application in vivo.[22-24] The existence of organic materials offers a strategy to modify the nanoparticles surface charge and chemical functionality for targeting therapeutic; at the same time, the introduction of organic materials can also inhibit the agglomeration and prolong their blood circulation time as stabilizing agents.

Among organic materials, natural polymer materials have been widely used in diverse areas for their superior properties such as hydrophilicity, nontoxicity, biocompatibility and biodegradability.[25,26] Carboxymethylcellulose (CMC) has become a well-known natural polymer material because of its unique physical and mechanical properties; in addition, the CMC molecules possess opposite electric charges and react strongly with some molecules due to the presence of carboxymethyl groups.[27-29] The nanocarriers are composed of magnetic nanoparticles modified with CMC have been successfully fabricated by various synthetic methods. Sahiner et al. reported magnetic carboxymethylcellulose particles via combining micro-emulsion polymerization with co-precipitation for drug delivery systems.[30] Sakthikumar et al. synthesized of carboxymethyl cellulose magnetic nanoparticles by two-step ionic cross-linking and in situ precipitation.[31] Barbucci et al. fabricated hybrid magnetic carboxymethylcellulose hydrogels for controlled doxorubicin release via cross-linking method.[32] Pilapong et al. designed carboxymethyl magnetic nanoparticles (CMC-MNPs) as a vehicle for drug delivery via modified chemical precipitation method.[33] Li et al. reported on the synthesis of the novel Fe$_3$O$_4$-carboxymethyl cellulose-5-fluorouracil (Fe$_3$O$_4$-CMC-5FU) nanomedicine by chemically bonding.[34] However, these approaches were of a general nature and not focused on the as-synthesized materials with narrow size distribution spherical and high magnetic moments; the processes were complex and required precision control. The performance in biological

a. Center for Biomedical Materials and Engineering, Harbin Engineering University, Harbin 150001, China.
b. Key Laboratory of Superlight Material and Surface Technology, Ministry of Education, Harbin Engineering University, Harbin 150001, China.
c. Department of Cardiology, Center of Vascular Diseases, Fourth Affiliated Hospital of Harbin Medical University, Harbin 150001, China.
E-mail: lrm1888@hotmail.com; lvweizhong@hrbeu.edu.cn;
Fax: +86 451 8253 3026; Tel: +86 451 8253 3026

New Journal of Chemistry Accepted Manuscript

applications was thus limited. Therefore, the development of a facile and economical synthetic method for producing the multi-functional magnetic carboxymethylcellulose nanomaterials would benefit their biomedical application.

5   In this study, we simplified the synthetic procedure of multi-functional magnetic carboxymethylcellulose (Fe_3O_4-CMC) nanomaterials which are composed of magnetic nanoparticles with abundant carboxyl groups on the interface by a facile one-step hydrothermal method. The as-prepared nanocarriers

10 exhibited excellent spherical shape and strong magnetic responsiveness, in comparison with other methods.[32, 33] The biocompatibility of Fe_3O_4-CMC nanocarriers was detected by a standard MTT cell assay with L929 cell lines. Consequently, we investigated the performance of the nanomaterials as drug

15 delivery carriers via loading DOX molecules. The Fe_3O_4-CMC nanocarriers can be easily conjugated with DOX molecules via electrostatic interaction due to the carboxyl groups on the surface which lead to high drug loading efficiency. Meanwhile, the release properties of DOX-loaded nanocarriers exhibited

20 excellent pH-responsive drug delivery to overcome the side-effects of DOX, such as instability at physiological pH and high cytotoxicity towards normal human cells.

Experimental

Materials

25 Carboxymethyl cellulose (CMC) was purchased from Tianjin Kermel Chemical Reagent Co., Ltd., China. Ferric chloride hexahydrate ($FeCl_3 \cdot 6H_2O$), ammonium acetate (NH_4Ac) and ethylene glycol in this work were purchased from Sinopharm Chemical Reagent Co., Ltd, China. All chemicals were used

30 without further purification.

Synthesis of Fe_3O_4-CMC nanocarriers

The magnetic nanocarriers were synthesized by a simple modified solvothermal reaction method: 0.675 g $FeCl_3 \cdot 6H_2O$ (2.5 mmol) as a precursor was dissolved in 35mL ethylene

35 glycol by stirring, followed by the addition of 1.925 g NH_4Ac (25 mmol). CMC with different composition ratios were added into the light brown suspension under continuous stirring to form a homogeneous solution. Subsequently, the solution was transferred and sealed in a Teflon-lined stainless-steel autoclave

40 (50 mL capacity) after stirring vigorously for 30 min. The autoclave was maintained at 200 ℃ for 12 h, and cooled to room temperature naturally. The black precipitate was collected by magnetic separation and washed with deionized water and absolute ethanol several times to effectively remove the solvent

45 before being dried in a vacuum at 60 ℃ for 24 h.

Characterization

The morphology and structure of the nanocarriers were characterized by a field emission scanning electron microscope (SEM, Hitachi S4800) and transmission electron microscope

50 (TEM, JEOL, JEM-2010). The size distribution of nanocarriers was determined by Nano Particle Size and Zeta potential analyzer (Malvern, Zetasizer Nano ZS90). The X-ray

diffraction (XRD) patterns were taken in a Rigaku D/max-IIIB diffractometer (Tokyo) using nickel-filtered Cu K_α radiation at

55 40 kV, 150 mA. X-ray photoelectron spectroscopy (XPS) measurements were performed using a PHI 5700 ESCA spectrometer with Al KR radiation (h_v= 1486.6 eV). Fourier-transform infrared (FTIR) spectra of the nanocarriers were recorded to analyze the surface characteristics of the

60 nanocarriers via an AVATAR 360 FTIR spectrophotometer in the 400–4000 cm^{-1} region by using the KBr-disk method. The magnetic properties of the nanocarriers were measured via vibrating sample magnetometry (VSM JDM-13) at room temperature. Thermogravimetric Analysis (TGA) was

65 performed on a NetzschSTA409 thermoanalyzer (Shimadzu Co.) from room temperature to 800 °C with a heating rate of 10 °C min^{-1} under a nitrogen atmosphere. The DOX concentration was carried out by UV–Vis (Shimadzu UV 1700) spectrophotometer.

Cells Cytotoxicity of Fe_3O_4-CMC nanocarriers

Typically, a MTT cell assay was performed to determine cell viability of the nanocarriers with the Vero cell line. L929 fibroblast cells were seeded onto 96-well plates with a density of 5000-6000 cells per well and incubated in DMEM medium

75 (0.1 mL) for 24 h to enable attachment of the cells to wells with 5% CO_2 at 37 °C. The naked Fe_3O_4 and Fe_3O_4-CMC nanocarriers were sterilized by ultraviolet irradiation for 2 h and added to the culture wells at different concentrations of 3.125, 6.25, 12.5, 25 and 50 μg mL^{-1}; meanwhile, the culture

80 wells without nanocarriers as the control groups. Then the solutions incubated for another 24 h at 37 °C with 5% CO_2. A total of 20 μL of MTT solution (5 mg/mL was prepared by PBS) was added to each well which contained different amounts of nanocarriers. Subsequently, the plate was incubated

85 for another 4 h and covered with aluminium foil for protection from light at 37 °C. In this period, viable cells facilitated a reduction of MTT to formazan, which can be dissolved by dimethyl sulfoxide (DMSO). After incubation, 100 μL of DMSO solution was added to each well and placed on a

90 shaking table for 5 min at 150 rpm to blend the formazan and solvent completely. The absorbance was measured by a microplate reader at 490 nm. Averages and standard deviations were performed in triplicate. The cell viability was calculated using the following equation:

$$\text{Cell viability (\%)} = \frac{A_{test}}{A_{control}} \times 100 \qquad (1)$$

95

where A_{test} is the average cell viability after adding the as-prepared nanocarriers; $A_{control}$ is the cell viability for the control experiment without nanocarriers.

Doxorubicin Loading and Release Test

100 Doxorubicin (DOX) was employed as a model drug. For DOX loading, the magnetic nanocarriers (30 mg) were dispersed into phosphate buffered saline (PBS) solution (5 mL) via ultrasound, and DOX (2 mg) was added into the solution. The mixture was slowly shaken for 24 h with an oscillator to

105 facilitate the loading of DOX molecules. The as-synthesized

solution was centrifugally separated at 6000 rpm for 4 min; meanwhile, the fresh PBS solution with a constant volume (5 mL) was replenished in the centrifugal tube and washed several times until the supernatant solutions kept colorless. Then the [5] supernatant solutions were collected and kept for UV−vis analysis.

The loading capacity (M_{LC}) and efficiency (LE%) were calculated using the following equation:

$$M_{LC} = \frac{M_{OD} - \sum M_{RD}}{M_S} \qquad (2)$$

[10]
$$LE(\%) = \frac{M_{OD} - M_{RD}}{M_{OD}} \times 100 \qquad (3)$$

where M_{OD} is the original DOX mass, M_{RD} is the residual DOX mass in the supernatant solutions and M_S is the nanocarriers mass.

A fresh PBS solution (5 mL) was replenished in the [15] centrifugal tube and kept shaken at 37 °C and 150 rpm with an oscillator. At a definite time interval, the tube was centrifuged at 6,000 rpm for 4 minutes and supernatant was stored at 4°C in the dark. The fresh PBS was replenished and kept a constant volume. PBS solutions were directly prepared with the pH [20] value of 5.0 and 7.4, respectively. The release efficiency of DOX-Loaded nanocarriers was determined using UV–Vis spectrophotometer.

Results and discussion

Synthesis and characterization of Fe$_3$O$_4$-CMC nanocarriers

[25] The detailed strategy for constructing Fe$_3$O$_4$-CMC nanomaterials and applying for drug carrier is described in the experimental part and schematically summarized in Scheme 1. The magnetic nanomaterials were prepared via hydrolysis and reduction of iron (III) chloride hexahydrate in ethylene glycol [30] at high temperature; in addition, CMC as the stabilizing agents modified the nanomaterials surface charge and chemical functionality. In the process of loading and releasing drugs, the drug molecules can be easily attached onto the surface of nanomaterials through electrostatic interaction and hydrogen [35] bonding, which can facilitate drug loading efficiency. Moreover, the drug-loaded nanocarriers could be targeted to the specific area under the application of an external magnetic field to
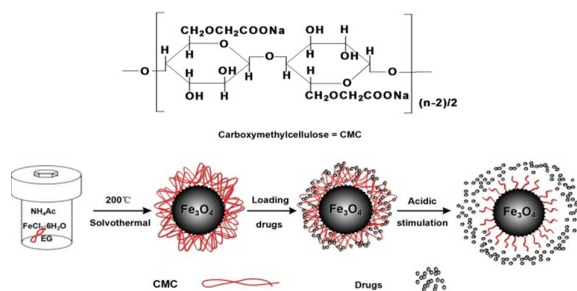
[40] **Scheme 1** Schematic for the formation mechanism of Fe$_3$O$_4$-CMC nanocarriers and subsequent loading and release of drugs in external pH system.
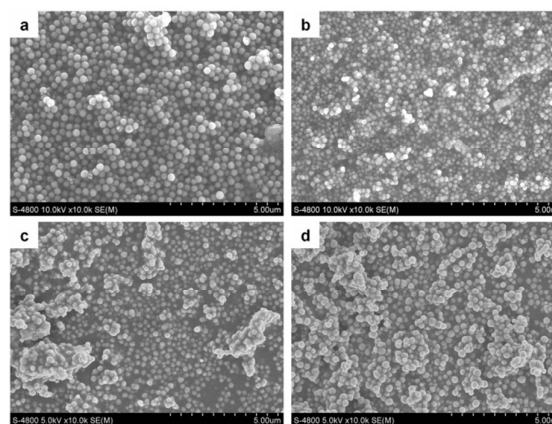
Fig. 1 SEM images of the naked Fe$_3$O$_4$ (a) and Fe$_3$O$_4$-CMC nanocarriers with different composition ratios (Fe^{3+}: CMC) 2: 1 (b); 1: 1(c); 1: 2 (d).

[45] improve drug release efficiency. To investigate the effect of composition ratios, the SEM images of Fe$_3$O$_4$-CMC nanocarriers with different amounts of CMC are shown in Fig. 1. Compared with naked Fe$_3$O$_4$ (Fig. 1a), the Fe$_3$O$_4$-CMC nanocarriers became smaller and kept uniformly spherical when [50] the weight ratio of Fe^{3+}: CMC was 2:1(Fig. 1b); however, the nanocarriers appeared spontaneously aggregate with increasing the weight ratio of Fe^{3+}: CMC from 1:1 to 1:2 (Fig. 1c and d) due to the crosslinking behaviour of CMC. The results suggest that the optimal composition ratio of Fe^{3+}: CMC is 2:1.

[55] From a further investigation of the morphology of Fe$_3$O$_4$-CMC nanocarriers, Fig. 2 shows SEM and TEM images of different magnification for both naked Fe$_3$O$_4$ without CMC and
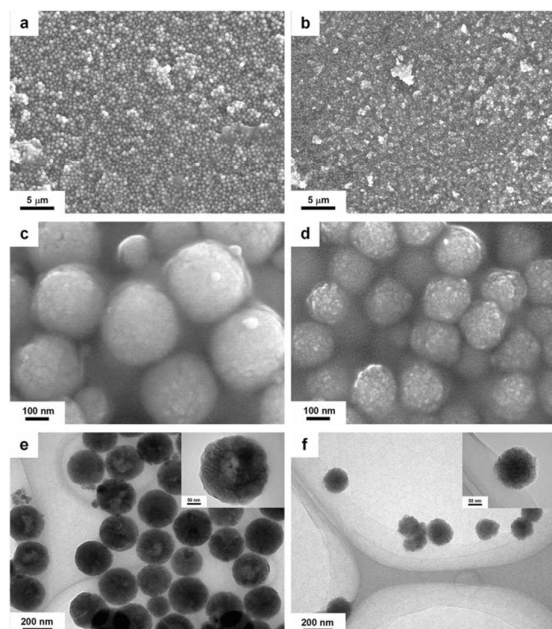
Fig. 2 SEM images of the naked Fe$_3$O$_4$ (a, c) and Fe$_3$O$_4$-CMC nanocarriers (b, d) with the [60] optimum composition ratio; TEM images of the naked Fe$_3$O$_4$ (e) and Fe$_3$O$_4$-CMC nanocarriers (f) with the optimum composition ratio.
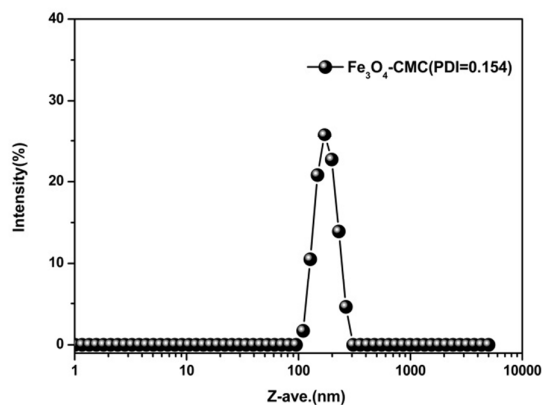
Fig. 3 Particle size distribution of Fe₃O₄-CMC nanocarriers with the optimum composition ratio.

Fe₃O₄-CMC nanocarriers with the optimum composition ratio. In contrast, the modified nanocarriers maintain an excellent spherical shape and exhibit a rough surface to facilitate the attachment of drug molecules onto the surface (Fig. 2b and d). Additionally, the key role of CMC in the formation of nanocarriers is demonstrated by TEM images. The hollow structure of naked Fe₃O₄ spheres is observed clearly in Fig. 2e, mainly due to thermal decomposition of NH_4Ac. The release of NH_3 bubbles along with the system's tendency to minimize interfacial energies, drives the self-assembly of the initial nanoparticles and the NH_3 bubbles are entrapped within nanocarriers.[35] We further observe from Fig. 2f, the Fe₃O₄-CMC nanocarriers become smaller and clearly composed of many small nanoparticles. This is due to the addition of CMC which expel the trapped NH_3 bubbles in the magnetic nanocrystals, which stabilize the formation of magnetic nanocrystals in the reaction. As shown in the insets of Fig. 2e and f, instead of a hollow structure, a rough and loose structural change becomes more distinct. Subsequently, the average diameter and size distribution of nanocarriers were also measured (Fig. 3). The average diameter size of Fe₃O₄-CMC
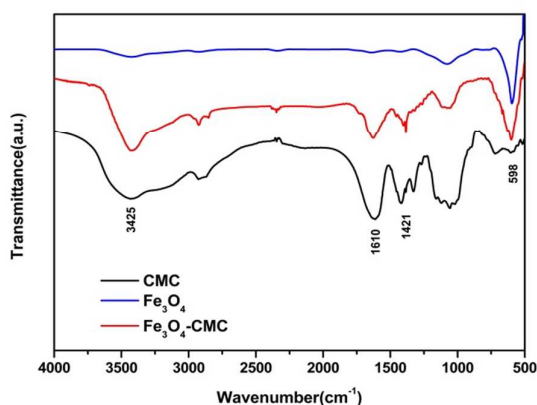

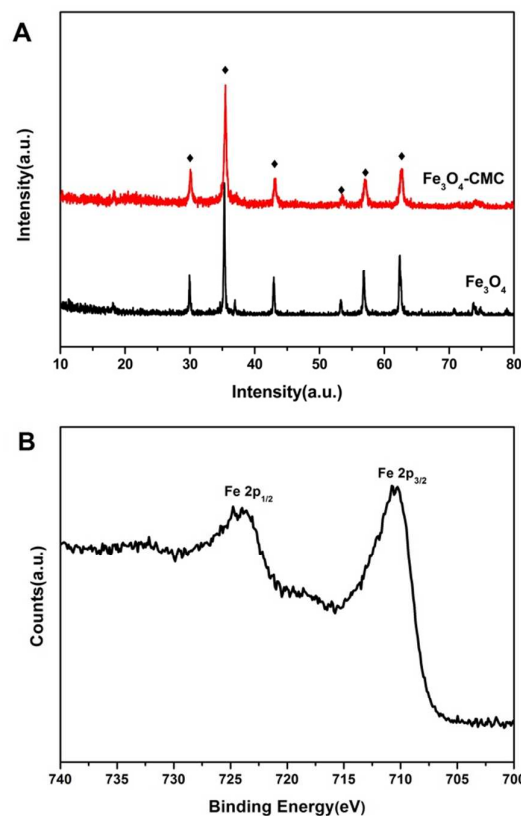**Fig. 4** FTIR spectra of nake Fe₃O₄; pure CMC and Fe₃O₄-CMC nanocarriers with the optimum composition ratio.

Fig. 5 XRD patterns (A) of the naked Fe₃O₄ and Fe₃O₄-CMC nanocarriers, and XPS spectrum (B) of Fe₃O₄-CMC nanocarriers with the optimum composition ratio.

nanocarriers is 147 nm and the polydispersity index is 0.154, which confirm the narrow size distribution of nanocarriers and fit well with SEM and TEM images. The result confirms that the rough-surfaced Fe₃O₄-CMC nanocarriers have been fabricated successfully and also indicates that the formed nanocarriers correspond to an ideal size for drug delivery applications.

The FTIR spectra of naked Fe₃O₄, pure CMC and Fe₃O₄-CMC nanocarriers are illustrated in Fig. 4, confirming the functional groups of as-synthesized nanocarriers. Compared with the spectrum of pure CMC, the nanocarriers demonstrate the existence of the hydroxyl, methyl and carboxyl groups: the –OH stretch is manifested through the peak of 3425 cm⁻¹; the characteristic absorption bands at 2925 cm⁻¹ and 2853 cm⁻¹ are related to stretching of C-H bonds in CH_2 groups; peaks at 1610 cm⁻¹ and 1421 cm⁻¹ are attributed to the $-COO^-$ symmetric stretch, respectively, corresponding to CMC structure.[36] From a comparison of the naked Fe₃O₄, the new peak at around 598 cm⁻¹ for Fe₃O₄-CMC nanocarriers is assigned to the characteristic absorption peak of Fe₃O₄. The spectra confirm that nanocarriers are successfully modified by CMC. The XRD spectra display a clear crystalline pattern to examine the effect of CMC on the crystal structure of synthesized nanocarriers in Fig. 5A. The six peaks (220) (311) (400) (422) (511) and (440) for naked Fe₃O₄ correspond to the peaks of pure Fe₃O₄ with

face-centred cubic structure (JCPDS Card No. 76‑1849).[37] The diffraction peaks intensity of Fe_3O_4-CMC nanocarriers becomes weaker than its corresponding naked Fe_3O_4 due to the introduction of CMC; however, the peak positions of Fe_3O_4-

5 CMC nanocarriers still match with the naked Fe_3O_4. Moreover, as seen in Fig. 5B, the XPS spectra exhibit peaks at 710.7 and 724 eV which are the characteristic peaks of $Fe_{2p}^{3/2}$ and $Fe_{2p}^{1/2}$ oxidation states, it gives further proof for the components of Fe_3O_4 nanoparticles.[38] The results are consistent with the above

10 TEM images and suggest that the addition of CMC do not change the crystal structure of Fe_3O_4.

Magnetization properties of as-synthesized samples are necessary for its practical application. The magnetic hysteresis curves (Fig. 6) of both samples were measured at 37 °C and

15 demonstrated that they are without remnant magnetization or coercivity, indicating that both samples are superparamagnetic at room temperature, which is characteristic of Fe_3O_4 nanoparticles.[39] It shows that the nanocarriers are composed of small magnetic nanoparticles, being consistent with the above

20 TEM images and XRD characterization. The saturation magnetization values is 62.1 emu g^{-1} for naked Fe_3O_4 and decreases to 54.6 emu g^{-1} for Fe_3O_4-CMC nanocarriers, which indirectly confirms the presence of polymer and further provides evidence for successful surface modification of

25 nanocarriers with CMC. The separation and redispersion of nanocarriers were also investigated (inset of Fig. 6). Clearly, all nanocarriers are attracted to the sidewall by applying an external magnet within 30s and redispersed quickly with slight shaking when the magnet is moved. It not only shows as-

30 prepared nanocarriers possess strong and rapid magnetic responsiveness, but also proves that magnetic nanocarriers can be adapted for practical bioapplications. Additionally, the fact of CMC anchored onto the nanocarriers is also confirmed by TGA curves in Fig. 7. The TG curves of the naked Fe_3O_4, pure

35 CMC and Fe_3O_4-CMC nanocarriers are illustrated for comparative data. The weight loss of naked Fe_3O_4 (7.4 wt. %) is mainly attributed to the removal of adsorbed water molecules and decomposition of organic matter introduced during the
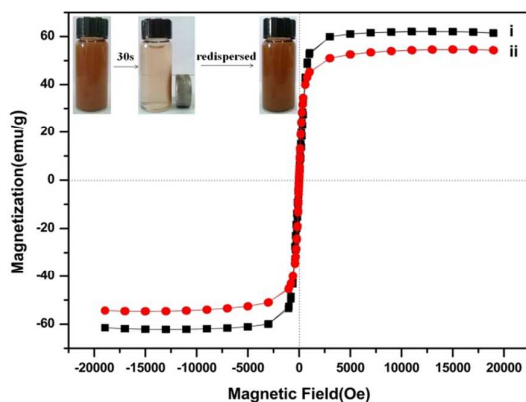

40 **Fig. 6** Magnetic hysteresis curves of the as-prepared naked Fe_3O_4 (i) Fe_3O_4-CMC nanocarriers (ii) with the optimum composition ratio. The inset shows photographs of in aqueous solution.
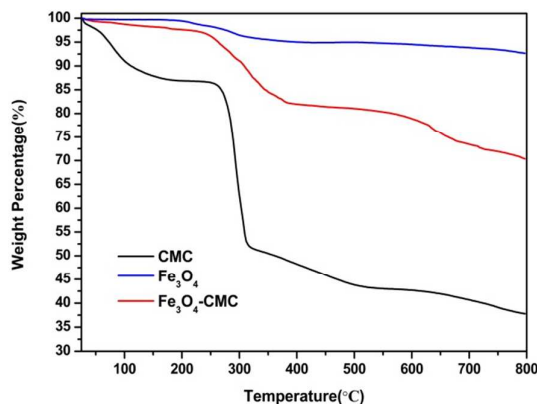

Fig. 7 TG curves of pure CMC; naked Fe_3O_4 and Fe_3O_4-CMC nanocarriers with the
45 optimum composition ratio.

hydrothermal process.[40] On the other hand, for pure CMC, the initial weight loss (13.4 wt. %) is associated with loss of water before 250°C for the hydrophilic CMC, and then a significant weight loss occurred around 250 °C due to the decomposition

50 of CMC.[41] Therefore, for Fe_3O_4-CMC nanocarriers, the initial weight loss (3.8 wt. %) at 30 – 250 °C is obtained due to the
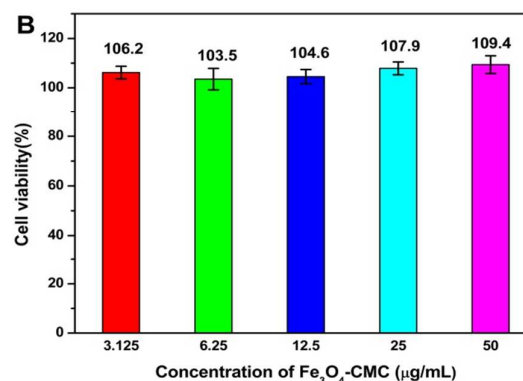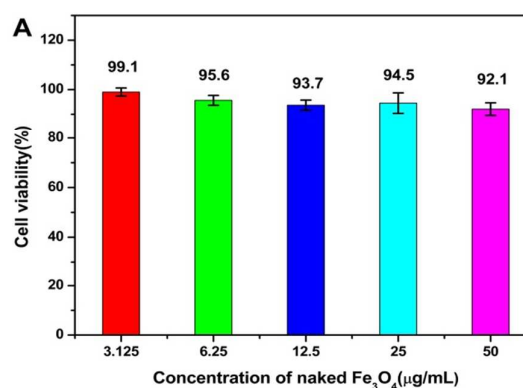

Fig. 8 Cell viabilities of naked Fe_3O_4 (A) and Fe_3O_4-CMC nanocarriers (B) with the optimum composition ratio to L929 cells measured by MTT assay.

evaporation of the different types of absorbed water molecules. Then the significant weight loss (25.7 wt. %) is mainly attributed to other organic matter introduced during the hydrothermal process and the decomposition of CMC which is successfully attached to the surface of the Fe_3O_4 nanoparticles. The results also explained that the magnetite content decreases with the addition of polymer and coherent with the above-mentioned discussion on VSM analyses.

In vitro cytotoxicity of Fe_3O_4-CMC nanocarriers

The cell viability of the nanomaterials is an important prerequisite and crucial factor for the actual application as a potential carrier in biomedical fields. Only nontoxic carriers are suitable for drug delivery. It has been reported that the magnetic materials exhibit no or low cytotoxicity in vivo.[17, 42] The as-prepared naked Fe_3O_4 and Fe_3O_4-CMC nanocarriers were incubated with L929 cell line and a standard MTT cell assay was used for the study (Fig. 8). As seen in Fig 8A, the cell viability is decreased to 92.1% with after 24 h treatment within the high-dosage concentrations of naked Fe_3O_4 (50 μg mL^{-1}); however, cell viability maintain more than 100% for the Fe_3O_4-CMC nanocarriers, indicated that the nanomaterials are nontoxic and the addition of CMC can decrease cytotoxicity to live cells. Therefore, the Fe_3O_4-CMC nanocarriers can potentially be applied as drug carriers for biological applications.

DOX release property of Fe_3O_4-CMC nanocarriers

DOX as a well-known anticancer drug is difficult to load from an aqueous medium due to the high water solubility.[43, 44] Recently, there are various studies to improve the DOX loading efficiency by cooperation of DOX with anionic polymers.[45, 46] Herein, DOX was selected to study drug storage and release properties of the Fe_3O_4-CMC nanomaterials as a potential candidate of drug carriers. During the loading and release process, the DOX molecules are attached onto the surface of nanomaterials through electrostatic interaction and hydrogen bonding and liberated by a diffusion-controlled mechanism. The carboxyl groups on the surface of nanocarriers are most likely the reactive sites that form hydrogen bonds with the DOX when it is attached with the surface. To further clarify the formation of the drug-loaded nanocarriers, the DOX-loaded nanocarriers were characterized by UV–vis spectroscopy in Fig 9A, compared with the results observed in bare Fe_3O_4-CMC nanocarriers and free DOX. As for DOX-loaded nanocarriers, there is a clear difference between the absorbance of the free DOX and bare nanocarriers. In addition, the drug loading capacity and efficiency were determined to be 61.7 mg g^{-1} and 92.5%, respectively. The loading efficiency is mostly attributed to electrostatic interaction and hydrogen bonding between the drug molecules and the nanocarriers, indicating further that the DOX molecules are loaded effectively onto the Fe_3O_4-CMC nanocarriers.

In addition, the cumulative drug release profiles of DOX-loaded nanocarriers are depicted in Fig. 9B. Here, pH values of 7.4 and 5.0 were selected to study the release properties, which
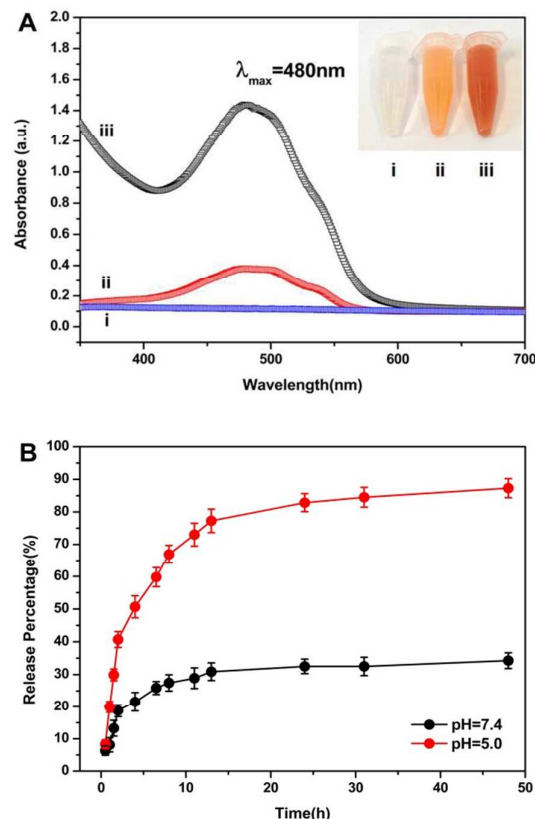

Fig. 9 Absorbance spectra (A) of bare Fe_3O_4-CMC nanocarriers (i), DOX-loaded nanocarriers (ii) and free DOX (iii), the inset shows related photographs of the supernatant solutions; Release profiles for DOX-loaded nanocarriers (B) with the optimum composition ratio at pH values 7.4 and 5.0.

were chosen as the biological blood environment and intracellular endosomal/lysosomal acidic environments inside a cancer cell, respectively. It is clearly observed the burst and sustained release steps from the release profiles. Surprisingly, the as-prepared DOX-loaded nanocarriers show an initial burst (18.8%) for 2 h due to the part of drug was absorbed onto the surface of nanocarriers and a sustained cumulative release (34.3%) followed up to 48 h in the physiological environment (pH =7.4), indicating that the stability of DOX-loaded nanocarriers does not significantly change during 48h. This is attributed to the interactions between the drug molecules and nanocarriers to restrict the release of DOX into aqueous medium. In addition, the DOX-loaded nanocarriers show a more rapid release (40.7%) for 2 h at pH 5.0 in comparison to the release at pH 7.4. After 48 h, the DOX sustained cumulative release as high as 87.3% via decreased the interactions between the drug molecules and nanocarriers, due to the carboxyl groups are mostly protonated and the solubility of DOX is increased in a more acidic environment.[47] The pH-responsive phenomenon is benefit for drug delivery due to the acidic extracellular and intracellular environments of tumors, which can accelerate drug release and offer sufficient cellular drug uptake or local drug concentration. Therefore, the data clearly support the use of

nanomaterials as promising smart carriers because it facilitates good stability of electrostatically bounding drug molecules in a normal physiological environment (normal tissue) and triggers release in a weakly acidic environment (solid tumors tissue). Moreover, the nanocarriers are helpful for selective targeting by an external magnetic field and enhancing the cell cytotoxicity of tumor cells. The nanomaterials, as an efficient multifunctional responsive delivery system, can greatly improve the therapeutic efficacy of drug.

Conclusions

In summary, the magnetic carboxymethylcellulose nanocarriers with dual responses were successfully synthesized via a facile one-step solvothermal method. The as-obtained nanocarriers show strong magnetic responsiveness and excellent spherical shape. In particular, there are abundant carboxyl groups on the surface of nanocarriers to which the doxorubicin molecules attach and show a high loading capacity and efficiency for bioapplication. The release profiles exhibit a remarkable pH-responsive of the nanocarriers, which maintain stability in blood circulation and sustained release drug at tumors tissue microenvironment, thus enhancing the therapeutic efficacy of the drug. We suggest that the as-prepared multifunctional nanomaterial is potentially promising in the drug release field.

Acknowledgements

Notes and references

1   Y. C. Chen, L. C. Liao, P. L. Lu, C. L. Lo, H. C. Tsai, C. Y. Huang, K. C. Wei, T. C. Yen and G. H. Hsiue, *Biomaterials*, 2012, **33**, 4576-4588.

2   Y. Wen, W. Liu, C. Bagia, S. J. Zhang, M. F. Bai, J. M. Janjic, N. Giannoukakis, E. S. Gawalt and W. S. Meng, *Acta Biomater.*, 2014, **10**, 4759-4767.

3   M. E. Fox, F. C. Szoka and J. M. J. Frechet, *Accounts Chem. Res.*, 2009, **42**, 1141-1151.

4   Y. Wen, H. R. Kolonich, K. M. Kruszewski, N. Giannoukakis, E. S. Gawalt and W. S. Meng, *Mol. Pharm.*, 2013, **10**, 1035-1044.

5   H. Wei, R. X. Zhuo and X. Z. Zhang, *Prog. Polym. Sci.*, 2013, **38**, 503-535.

6   J. Nicolas, S. Mura, D. Brambilla, N. Mackiewicz and P. Couvreur, *Chem. Soc. Rev.*, 2013, **42**, 1147-1235.

7   H. H. Xiao, G. T. Noble, J. F. Stefanick, R. G. Qi, T. Kiziltepe, X. B. Jing and B. Bilgicer, *J. Control. Release*, 2014, **173**, 11-17.

8   D. Zhou, H. Xiao, F. Meng, X. Li, Y. Li, X. Jing and Y. Huang, *Adv. Healthc. Mater.*, 2013, **2**, 822-827.

9   R. Cheng, F. Meng, C. Deng, H.-A. Klok and Z. Zhong, *Biomaterials*, 2013, **34**, 3647-3657.

10 S. Mura, J. Nicolas and P. Couvreur, *Nat. Mater.*, 2013, **12**, 991-1003.

11 A. Balducci, Y. Wen, Y. Zhang, B. M. Helfer, T. K. Hitchens, W. S. Meng, A. K. Wesa and J. M. Janjic, *Oncoimmunology*, 2013, **2**.

12 L. K. Bogart, G. Pourroy, C. J. Murphy, V. Puntes, T. Pellegrino, D. Rosenblum, D. Peer and R. Levy, *ACS Nano*, 2014, **8**, 3107-3122.

13 A. K. Pal, I. Aalaei, S. Gadde, P. Gaines, D. Schmidt, P. Demokritou and D. Bello, *ACS Nano*, 2014, **8**, 9003-9015.

14 N. Erathodiyil and J. Y. Ying, *Accounts Chem. Res.*, 2011, **44**, 925-935.

15 K. E. Sapsford, W. R. Algar, L. Berti, K. B. Gemmill, B. J. Casey, E. Oh, M. H. Stewart and I. L. Medintz, *Chem. Rev.*, 2013, **113**, 1904-2074.

16 H. Xiao, J. F. Stefanick, X. Jia, X. Jing, T. Kiziltepe, Y. Zhang and B. Bilgicer, *Chem. Commun.*, 2013, **49**, 4809-4811.

17 J. J. Wang, C. Gong, Y. N. Wang and G. L. Wu, *Colloids Surf. B-Biointerfaces*, 2014, **118**, 218-225.

18 M. Mahmoudi, S. Sant, B. Wang, S. Laurent and T. Sen, *Adv. Drug Deliv. Rev.*, 2011, **63**, 24-46.

19 M. Colombo, S. Carregal-Romero, M. F. Casula, L. Gutierrez, M. P. Morales, I. B. Boehm, J. T. Heverhagen, D. Prosperi and W. J. Parak, *Chem. Soc. Rev.* 2012, **41**, 4306-4334.

20 G. Wang, L. Jin, Y. Dong, L. Niu, Y. Liu, F. Ren and X. Su, *New J. Chem.*, 2014, **38**, 700-708.

21 L. Zhu, D. Wang, X. Wei, X. Zhu, J. Li, C. Tu, J. Su, J. Wu, B. Zhu and D. Yan, *J. Control. Release*, 2013, **169**, 228-238.

22 O. Veiseh, J. W. Gunn and M. Zhang, *Adv. Drug Deliv. Rev.*, 2010, **62**, 284-304.

23 L. H. Reddy, J. L. Arias, J. Nicolas and P. Couvreur, *Chem. Rev.*, 2012, **112**, 5818-5878.

24 J. Xie, G. Liu, H. S. Eden, H. Ai and X. Chen, *Accounts Chem. Res.*, 2011, **44**, 883-892.

25 S. Mizrahy and D. Peer, *Chem. Soc. Rev.*, 2012, **41**, 2623-2640.

26 N. Lin, J. Huang and A. Dufresne, *Nanoscale*, 2012, **4**, 3274-3294.

27 M. J. Ernsting, M. Murakami, E. Undzys, A. Aman, B. Press and S.D. Li, *J. Control. Release*, 2012, **162**, 575-581.

28 M. J. Ernsting, W. D. Foltz, E. Undzys, T. Tagami and S.D. Li, Biomaterials, 2012, **33**, 3931-3941.

29 M. J. Ernsting, W.-L. Tang, N. MacCallum and S.D. Li, *Bioconjugate Chem.*, 2011, **22**, 2474-2486.

30 S. Butun, F. G. Ince, H. Erdugan and N. Sahiner, *Carbohyd. Polym.*, 2011, **86**, 636-643.

31 B. Sivakumar, R. G. Aswathy, Y. Nagaoka, M. Suzuki, T. Fukuda, Y. Yoshida, T. Maekawa and D. N. Sakthikumar, *Langmuir*, 2013, **29**, 3453-3466.

32 R. Barbucci, G. Giani, S. Fedi, S. Bottari and M. Casolaro, *Acta Biomater.*, 2012, **8**, 4244-4252.

33 C. Pilapong, Y. Keereeta, S. Munkhetkorn, S. Thongtem and T. Thongtem, *Colloids Surf. B-Biointerfaces*, 2014, **113**, 249-253.

34 X. K. Liu, X. Deng, X. H. Li, D. S. Xue, H. L. Zhang, T. Liu, Q. F. Liu, N. J. Mellors, Y. M. Li and Y. Peng, *Nanomedicine*, 2014, **9**, 1389-1402.

35 B. Luo, S. Xu, A. Luo, W.-R. Wang, S.-L. Wang, J. Guo, Y. Lin, D.-Y. Zhao and C.-C. Wang, *ACS Nano*, 2011, **5**, 1428-1435.

36 A. M. Grumezescu, E. Andronescu, A. Ficai, C. Bleotu, D. E. Mihaiescu and M. C. Chifiriuc, *Int. J. Pharm.*, 2012, **436**, 771-777.
37 C. H. Li, R. X. Wei, Y. M. Xu, A. L. Sun and L. H. Wei, *Nano Res.*, 2014, **7**, 536-543.
38 S. M. Zhu, J. J. Guo, J. P. Dong, Z. W. Cui, T. Lu, C. L. Zhu, D. Zhang and J. Ma, *Ultrason. Sonochem.*, 2013, **20**, 872-880.
39 X. J. Kang, Y. L. Dai, P. A. Ma, D. M. Yang, C. X. Li, Z. Y. Hou, Z. Y. Cheng and J. Lin, *Chem. Eur. J*, 2012, **18**, 15676-15682.
40 S. Zhang, Y. Zhou, W. Nie and L. Song, *Cellulose*, 2012, **19**, 2081-2091.
41 W. Li, B. J. Sun and P. Y. Wu, *Carbohyd. Polym.*, 2009, **78**, 454-461.
42 L. Zang, J. Qiu, X. Wu, W. Zhang, E. Sakai and Y. Wei, *Ind. Eng. Chem. Res*, 2014, **53**, 3448-3454.
43 X. Ma, H. Tao, K. Yang, L. Feng, L. Cheng, X. Shi, Y. Li, L. Guo and Z. Liu, *Nano Res.*, 2012, **5**, 199-212.
44 W. She, N. Li, K. Luo, C. Guo, G. Wang, Y. Geng and Z. Gu, *Biomaterials*, 2013, **34**, 2252-2264.
45 X. Feng, F. Lv, L. Liu, H. Tang, C. Xing, Q. Yang and S. Wang, *ACS Appl. Mater. Interfaces*, 2010, **2**, 2429-2435.
46 K. H. Min, H. J. Lee, K. Kim, I. C. Kwon, S. Y. Jeong and S. C. Lee, *Biomaterials*, 2012, **33**, 5788-5797.
47 T. Zhang, G. Y. Li, L. Guo and H. Chen, *Int. J. Biol. Macromol.*, 2012, **51**, 1109-1115.

The multi-functional magnetic carboxymethylcellulose nanocarriers were successfully synthesized via a facile solvothermal method.